Steady-State Relative Permeability Measurements of Tight and Shale Rocks Considering Capillary End Effect

Steady State Relative Permeability Measurements of Tight and Shale Rocks Considering Capillary End Effect

Rasoul Nazari Moghaddam, Mahmoud Jamiolahmady

Institute of Petroleum Engineering, School of Energy, Geoscience, Infrastructure and Society, Heriot-Watt University

Abstract

Relative permeability (k_r) data are the key factors for describing the behaviour of the multiphase flow in porous media. During the k_r measurements of low permeability rocks, high capillary pressure can cause a significant liquid hold-up at the core outlet. This liquid hold-up, which is known as Capillary End Effect (CEE) is the main difficulty for laboratory measurements of relative permeability (k_r) for tight and shale rocks. In this paper, a novel method is proposed to correct the CEE during the steady-state relative permeability (SS k_r) measurements. The integrity of the proposed method is evaluated by a set of artificially generated data and the experimental SS- k_r data of an Eagle Ford shale sample. It is shown that accurate k_r data can be obtained using the proposed technique. This technique can be used to estimate reliable k_r data without any saturation profile measurement equipment, such as CT-scan or MRI.

Keywords

relative permeability; shale rock; capillary end effect; unconventional reservoirs; steady state

1. Introduction

Relative permeability (k_r) functions are among the required data for simulation of multiphase flow in porous media. Such data are crucial for the estimation of productivity, ultimate recovery, formation injectivity and planning various engineering operations, including EOR and diagnosing formation damage [1, 2].

Relative permeability data are usually measured in the laboratory using different techniques, including centrifuge, steady state, and unsteady state displacements. In a steady-state displacement, a constant total flow rate of liquid and gas is usually injected, while their ratio can be changed. In steady state method, it is necessary to reach to the equilibrium state across the core. After equilibrium, the pressure drop and flow rate data

are used to calculate the individual phase k_r values, according to Darcy's law. Among the methods developed for k_r measurements, the most reliable technique is the steady state method [3, 4]. In this technique, k_r curves can be determined for a wider range of saturation compared to the other methods. However, this method has some disadvantages, including the long time required to attain the steady state and the capillary end effects [5, 6]. Nevertheless, considering the non-uniqueness and unreliability of the results obtained by the other techniques, the steady state method is still the most reliable one for relative permeability measurements.

Relative permeability measurements of unconventional rocks are much more difficult compared to k_r measurements of conventional rock samples. In unconventional rocks, the capillary pressure is significantly high compared to conventional matrix. In fact, the capillary pressure increases as the average pore size of the system decreases. In low-permeability unconventional rocks, the average size of pores/throats is much smaller than the average pore size in conventional rocks. Thus, higher capillary pressure is expected in the unconventional rocks. Results of MICP measurements (mercury intrusion capillary pressure) performed on shale samples showed great capillary pressure, up to 70,000 psi [7, 8]. Such high capillary pressure can influence the two-phase flow in unconventional rocks. For example, during the relative permeability measurements, high capillary pressure can cause a significant liquid hold-up at the core outlet. This liquid hold-up, which is known as Capillary End Effect (CEE) is the main difficulty for laboratory measurements of relative permeability (k_r) for tight and shale rocks. In other words, as the capillary pressure is significantly high in the unconventional porous media, the CEE is dominant that makes all k_r measurements, incorrect and unreliable [9].

Liquid hold-up (or CEE) is generally created due to a discontinuity in capillary pressure at the core outlet. This discontinuity causes an accumulation of wetting phase at the end part of the core. As a result, the saturation distribution of the wetting phase along the core is not uniform, which influences the pressure drop and the calculated k_r. Figure 1 shows a schematic of the saturation profile inside a core sample with a CEE region at the outlet. It should be noted that the main problem for the study of end effect is determination of the liquid saturation profile along the core. As mentioned, CEEs are more significant in tight/shale rock samples compared to the conventional rocks, because the capillary pressure is higher in the unconventional tight formations. One of the practical solutions to overcome the CEE during the k_r measurements is to increase

the injection rate or the core length. Although this may not be always possible for unconventional rocks, because of their low/ultralow matrix permeability which causes significant pressure drop and longer equilibrium time. Therefore, the capillary end effect may cover most of the core length during the steady state displacements. It happens because the length of the CEE region depends on the competition of the capillary and viscous forces. In other words, a lower rate (i.e. low viscous force) in a porous medium with high capillary pressure results in a longer CEE length.

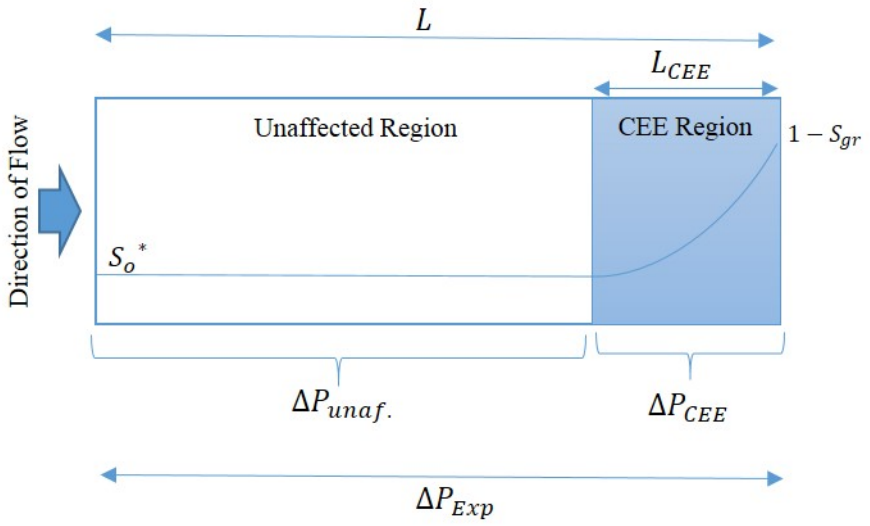

Figure 1 : A schematic of saturation profile of the wetting phase inside the core during the steady state relative permeability measurement when the capillary end effect (CEE) is dominant.

The capillary end effect has been extensively studied for many years. Leverett (1941) mentioned the boundary effect in porous materials [10]. Osoba et al. (1951) reported that there is no variation in k_r at different rates in the absence of boundary effects [11]. They proposed using high flow rates to minimise the end effects. Rapaport and Leas (1953) studied effects of the core length and injection rate on the flooding behaviour. They concluded that the same flooding behaviour is obtained for different lengths, if the injection rates are properly adjusted. They added that the flooding behaviour dependency to the rate and length decreases as anyone of these factors increases in value. They also proposed a scaling criteria to determine the stabilisation of flooding [12].

In addition, there are several published papers, which propose that additional information should be obtained (e.g. in-situ saturation, independent measurement of capillary pressure, in-situ pressure measurements along the core) to correct measured relative permeability data for CEE. Haung and Honarpour (1988) proposed the use of

k_r-P_c relationships to correct the capillary end effects. However, their method is difficult to apply and may not be valid for rocks with unknown k_r-P_c functions [13]. Qadeer et al. (1991) developed a model, which consists of an optimisation algorithm to estimate the oil/water k_r exponential functions from the unsteady state displacement experiments. However, in this approach, a P_c function is required and the match might not be unique [14]. Virnovsky et al. (1995, 1998) proposed measuring P_c separately, which is then used to estimate saturation and k_r data and correct CEE [6, 15]. Chen and Wood (2001) measured the in-situ saturation and pressure at different intervals along the core. Although during the k_r measurements the pressure can be recorded by internal taps, it is expensive and impractical for cores such as shale and tight samples, which are not long enough [16].

It is noted that all the studies mentioned above have been performed on conventional core samples. Recently, Gupta and Maloney (2015) proposed a technique to correct CEE by performing measurements at different flow rates. Although no additional information (e.g. in-situ saturation) is required in their method, they assumed a constant wetting phase k_r along the core, which is open to question. In addition, they did not consider the variation of the length of the CEE region at different flow rates [9]. In this paper, this issue is discussed in detail and it is shown that the length of the CEE region is not constant and changes with the flow rate, which poses serious questions on the validity of the approach proposed by Gupta and Maloney (2015).

As indicated above, in most of the proposed methods for CEE correction, additional information such as in-situ saturation or in-situ pressure is required. In practice, it is difficult to have an in-situ pressure transducer on shale/tight samples, which are general small plugs. It is noted that the length of the shale/tight rock samples used in the displacement experiments are generally small, due to the ultralow permeability of these rock types. In addition, measurements of in-situ liquid saturation are very expensive and may not be accurate for such small samples. To date, there is no reported data on relative permeability measurements of shale rock samples corrected for capillary end effects. The previous theoretical and experimental studies were developed for conventional rock types. To the best of the author's knowledge, this is the first time that the relative permeabilities of shale samples have been measured, and the capillary end effects have been corrected, based on a proposed unique method.

In this paper, the results of measuring relative permeability of an Eagle Ford shale sample are presented. To handle the CEEs, a new technique has been proposed to

correct the experimental k_r data. In this method, four different flow rates are required to be injected for each flow rate ratio. For all flow rates, the pressure drop across the core and the measured wetting phase saturations (obtained by material balance) are used to solve the four pressure and four saturation equations simultaneously. From the results, the CEE length at each flow rate, corrected wetting phase saturation, average wetting phase saturation in the CEE region and the corresponding k_r values can be obtained. It should be noted that, the correction of the k_r data means that more accurate values are obtained through the modification of k_r calculations. In other words, by this correction, the influence of CEE can be removed during the SS k_r measurements. To examine the integrity of the proposed method, two theoretically generated data sets were used. The results obtained from this technique were compared with the original k_r input data to evaluate the prediction error. In addition, as will be discussed in the last part of the paper, the proposed technique has been applied to the experimental data, from measurements performed on an Eagle Ford shale sample to obtain the actual k_r functions.

2. Experiments: Materials and Method

The steady state relative permeability (SS-k_r) experiments were performed on an Eagle Ford shale sample. The basic properties of this shale rock sample are shown in Table 1. The rock sample was dried overnight at 105 ℃ while connected to the vacuum pump. The absolute permeability of the Eagle Ford is 9.9 μD at net stress of 1000 psi (assuming an effective stress coefficient of unity). The absolute permeability of the rock sample was measured using pure N_2 and corrected for slippage effects. The details of the measurements and corrections can be found elsewhere [22]. For these measurements, a fluid system of Butane/Nitrogen (C_4/N_2) at 1500 Psi and 22 ℃ was used. The fluid PVT properties were obtained using PVTi - Eclipse Software. The interfacial tension (IFT) of the system was estimated as 5.5 mN/m under the experimental conditions. This fluid system (with low viscosities) was intentionally selected to minimise the pressure difference across the core. For fluid preparation, pure nitrogen (N_2) and butane (C_4) were mixed in the recombination cell and shaken for 24 hours to reach the equilibrium state. The overall molar compositions of the N_2 and C_4 were 40% and 60%, respectively. The fluids were mixed based on the calculated volume at 1500 psi using PVTi - Eclipse Software. After equilibrium, the liquid and gas were separated into gas and liquid injection cells.

The imbibition SS-k_r measurements were performed by co-injection of liquid and gas into the gas saturated core. The schematic diagram of the steady state setup is shown in Figure 2. The pressures were measured across the core at the inlet and outlet using a Quartzdyne pressure transducer. The accuracy of these pressure transducers is ±0.015% FS. Four accurate Quizix pumps were used at the same time for fluid injection and retraction. Prior to each experiment, a gas leakage test at high pressure was performed on the system. In addition, the dead volumes of all lines and valves were measured based on the Boyle two-cell method, using nitrogen at low pressure. The measured dead volume was double-checked by using a standard core, which had a known pore volume of 0.4 cc.

The liquid and gas were injected simultaneously through the core and continued to reach the equilibrium state. It is noted that the core was saturated by N_2 before simultaneous injection of N_2 and C_4. Gas and liquid were injected into the core at the selected value of LGR (liquid to gas ratio, volume liquid/volume gas, at test conditions). The equilibrium state was achieved when the rate of gas and liquid injection was equal to rate of gas and liquid retractions. In addition, the pressure drop across the core sample was stable when the steady state condition was achieved. Then, the average saturation of the core was calculated based on an accurate material balance, benefiting from the HPHT visual separator, which enabled the gas and liquid production to be measured at test conditions. In other words, the error caused by fluid expansion/contraction was removed when the measurements were performed under the experimental conditions. Furthermore, since the pore volumes of shale samples are generally low, the material balance calculations are subject to significant error without accurate measurement of fluid production. The accuracy of the visual separator used in this study was ±0.07 cc, which allows an error of <1% for saturation measurements. Finally, the recorded pressure drop was used in Darcy's law to obtain relative permeability values for both liquid and gas phases. For each fractional flow, the total flow rates of 10 cc/hr (1.6 m/day), 13 cc/hr (2.1 m/day), 16 cc/hr (2.5 m/day) and 20 cc/hr (3.2 m/day) were injected.

After each measurement, to restore the initial conditions, the core was left at atmospheric pressure and room temperature overnight. In addition, the core was cleaned by injection of several pore volumes methane to remove any remained liquid butane. The core absolute permeability was measured before each test to ensure that the original conditions had been restored. It is noted that the experiments were not conducted in

sequence. In other words, for each injection rate (at each LGR), the initial condition was established, and the simultaneous co-injection was performed.

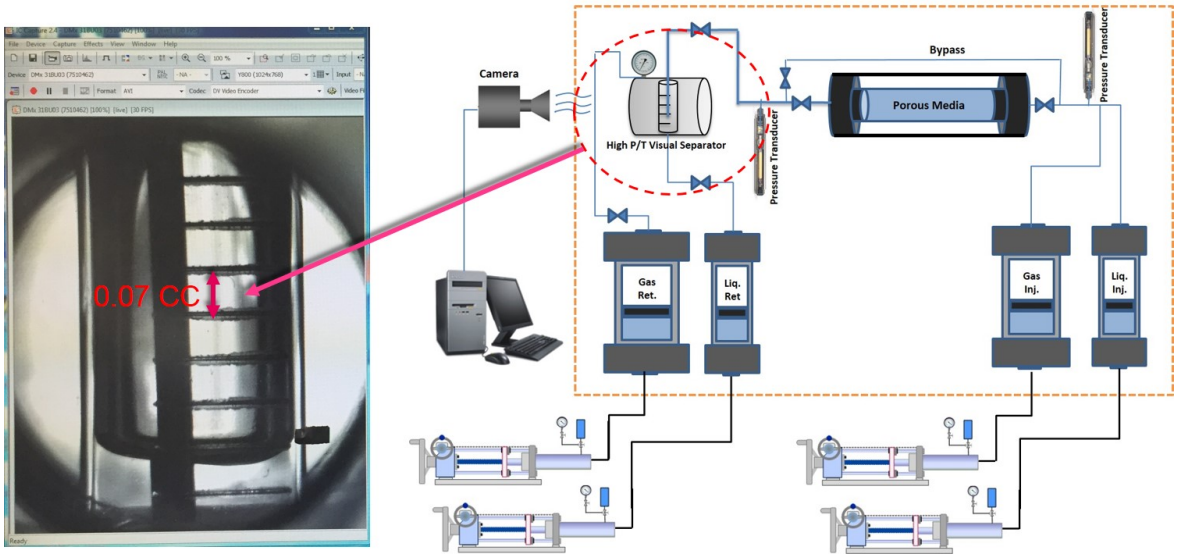

Figure 2 : The schematic diagram of the steady state relative permeability measurement setup equipped with a high-pressure visual separator with an accuracy of 0.07 cc.

Table 1 : Basic properties of the shale rock sample used in this study.

Shale Sample	Length (cm)	Diameter (cm)	Porosity (%)	Abs. Permeability (μD)	Orientation	Moisture
Eagle Ford	4.61	3.77	13.5	9.9	Parallel to bedding	Fully Dry

3. Multi-Rate Method for Capillary End Effect Correction

Capillary End Effect for SS Displacement

For the first time, Richardson et al. (1952) used the capillary end effect formulation in two immiscible fluid injection into horizontal porous media. They have conducted a series of gas-displacing-oil experiments using a Berea sandstone to study capillary end effects. Richardson et al. compared their experimental results with the obtained analytical solutions and demonstrated excellent agreements between measurements and predictions [5]. Later, Huang and Honarpour (1998) used the same formulation to discuss an experiment of co-injecting oil and water into a water pre-saturated, water-wet core sample. They used capillary end effect formulation in steady state displacement to

show how the relative permeability and capillary pressure can be estimated from the non-uniform liquid saturation profile. In the following, same formulation was used to obtain the liquid saturation profile when capillary end effects are not negligible [13].

In a SS-k_r measurement experiment, assuming incompressible and immiscible fluids, the following equations can be used for one-dimensional flow of gas and liquid (oil), including the capillary pressure:

$$q_g = \frac{-Kk_{rg}A}{\mu_g}\frac{\partial P_g}{\partial x} \tag{1}$$

$$q_o = \frac{-Kk_{ro}A}{\mu_o}\frac{\partial P_o}{\partial x} \tag{2}$$

$$P_c = P_g - P_o \tag{3}$$

The gradient of capillary pressure can be stated as:

$$\frac{\partial P_c}{\partial x} = \frac{1}{KA}\left(\frac{q_o\mu_o}{k_{ro}} - \frac{q_g\mu_g}{k_{rg}}\right) \tag{4}$$

and

$$\frac{\partial P_c}{\partial x} = \frac{dP_c}{dS_o}\frac{\partial S_o}{\partial x} \tag{5}$$

$$\frac{1}{KA}\left(\frac{q_o\mu_o}{k_{ro}} - \frac{q_g\mu_g}{k_{rg}}\right) = \frac{dP_c}{dS_o}\frac{\partial S_o}{\partial x} \tag{6}$$

Hence at steady state conditions:

$$dx = \frac{\frac{dP_c}{dS_o}\,dS_o}{\frac{1}{KA}\left(\frac{q_o\mu_o}{k_{ro}} - \frac{q_g\mu_g}{k_{rg}}\right)} \tag{7}$$

The above equation can be integrated along the core from x to L, i.e. from S_o to $1 - S_{gr}$ [17]:

$$x = L - KA\int_{S_o}^{1-S_{gr}} \left[\frac{\frac{dP_c}{dS_o}}{\left(\frac{q_o\mu_o}{k_{ro}} - \frac{q_g\mu_g}{k_{rg}}\right)}\right] dS_o \tag{8}$$

It should be noted that S_{gr} is the residual gas saturation, which is assumed to be constant. The saturation profile along the core can be obtained analytically from the above equation if the capillary pressure and relative permeability functions are known. It is noted that the reliability of this equation were confirmed before [5]. As an example,

for the application of this equation, it was used with known P_c and k_r data (shown in Figure 3) to produce a typical saturation profile. Figure 4 shows a theoretical saturation profile generated by Equation 8 for two different flow rates at the same liquid/gas flow rate ratio (F or LGR). As shown in this Figure, by increasing the flow rate, the length of the CEE region is decreased and the effect of the boundary is reduced. Hence, various flow rates give different CEE lengths (L_{CEE}). This solution clearly supports the conclusion that, at higher flow rates, the CEE is reduced. In addition, it is shown that the wetting phase (liquid) saturation ($S_o{}^*$) in the unaffected region of the core is not influenced by the capillary end effect and it is the same at both flow rates: i.e. at the same flow rate ratio (F), the wetting phase saturation in the unaffected zone is constant and independent of the flow rates. In this study, these two regions (unaffected and CEE) will be used later in the proposed method to capture CEEs during SS-k_r measurements.

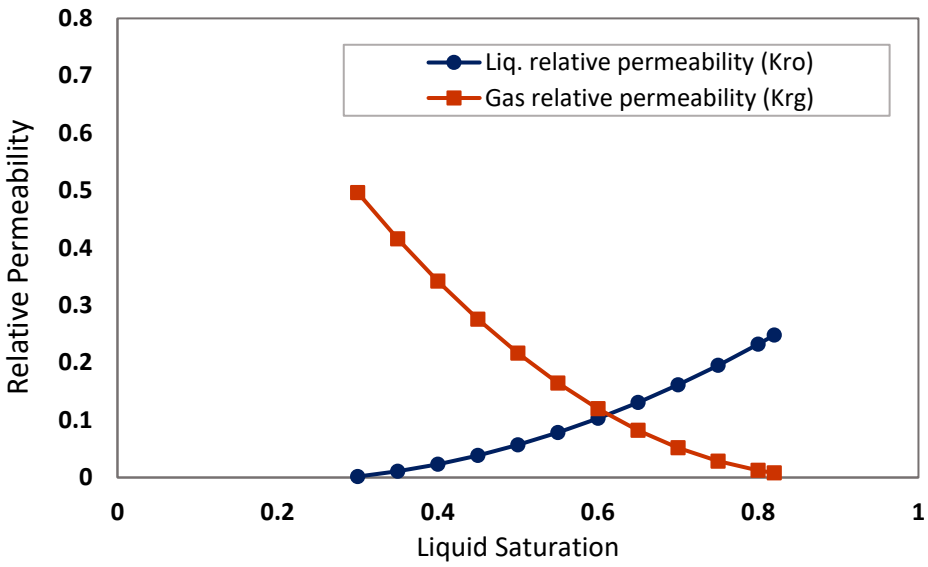

(a)

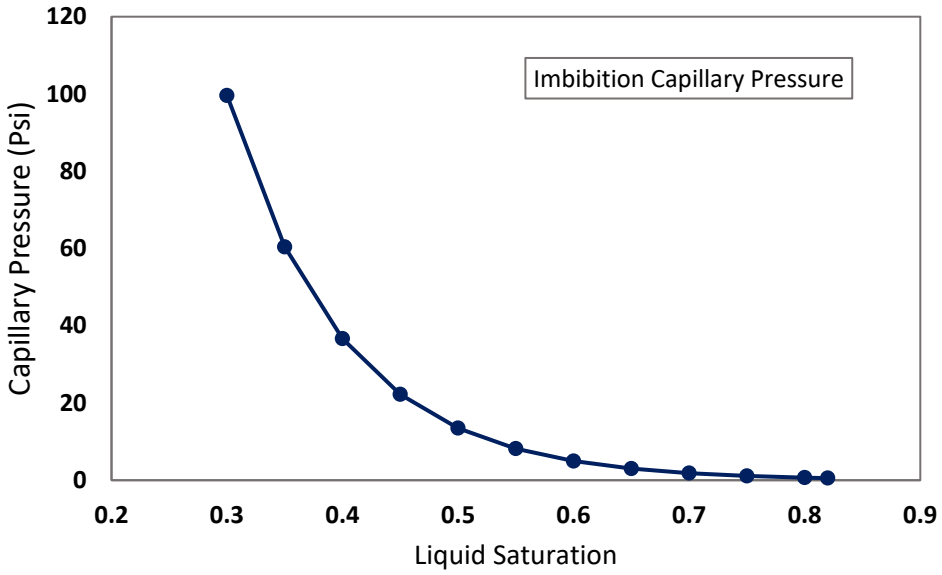

(b)

Figure 3 : (a) Imbibition relative permeability and (b) imbibition capillary pressure data used in the analytical solution.

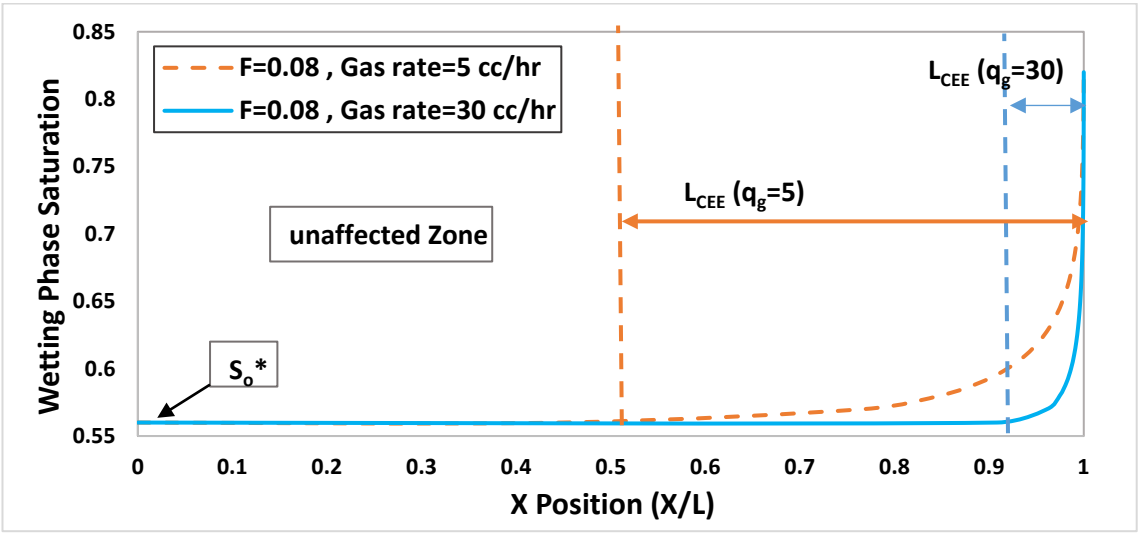

Figure 4 : Theoretical wetting phase saturation profile for constant LGR of 0.08 and at different gas flow rates of 5 and 30 cc/hr.

Method Development

In the steady state relative permeability (SS-k_r) measurements, the saturation profile can give valuable information regarding the capillary end effect (CEE). Among available techniques for the determination of saturation profile, the X-ray computed tomography method (X-ray CT) is the most popular one [18-20]. Magnetic resonance imaging

(MRI) is also a well-established method for such purposes [21]. In the steady-state experiments, the measured saturation profile together with a pre-determined P_c function can be used to obtain the SS-k_r data using a history matching technique. However, the SS-k_r values obtained may not be unique. In addition, obtaining saturation profile measurements with the current techniques make the experiment more complicated and expensive. In the method proposed in this study, only a conventional steady state setup is required with no additional modifications. In this technique, data of different rates are needed for each fractional flow, to correct SS-k_r and saturation data obtained from the experiments.

As explained previously, the saturation profile along the core can be divided into two separate regions of CEE and unaffected zone. In the unaffected zone, the wetting phase saturation is constant while in the CEE region, the wetting phase saturation changes from the S_o^* to $(1 - S_{gr})$, where S_{gr} is the residual gas saturation. It is noted that the k_r data is constant in the unaffected zone, as it is only a function of fluid saturation, which is constant in that region.

In addition, knowing the saturation profile along the core, the gas pressure drop can be calculated as follows:

$$\int dP_g = \frac{q_g \mu_g}{KA} \int \frac{dx}{k_{rg}} \tag{9}$$

For the CEE region, the pressure drop can be obtained as:

$$\int_{P_{L_{CEE}}}^{P_{out}} dP_g = \frac{q_g \mu_g}{KA} \int_{L_{CEE}}^{L} [\frac{dx}{k_{rg}(S_o)}] \tag{10}$$

Using Equation 7, gives:

$$\int_{P_{L_{CEE}}}^{P_{out}} dP_g = \frac{q_g \mu_g}{KA} \int_{S_o^*}^{1-S_{gr}} [\frac{\left[\frac{\frac{dP_c}{dS_o}}{\frac{1}{KA}(\frac{q_o \mu_o}{k_{ro}} - \frac{q_g \mu_g}{k_{rg}})}\right]}{k_{rg}(S_o)}] dS_o \tag{11}$$

After some manipulations it gives:

$$\Delta P_{CEE} = \int_{S_o^*}^{1-S_{gr}} \frac{\frac{dP_c}{dS_o} dS_o}{(F \frac{\mu_o k_{rg}}{\mu_g k_{ro}} - 1)} \tag{12}$$

where F is the liquid gas flow rate ratio (LGR):

$$F = \frac{q_o}{q_g} \tag{13}$$

As mentioned before and shown in Figure 4, in the CEE region the wetting phase saturation changes from $S_o{}^*$ at the beginning to $(1 - S_{gr})$ at the end of the core. From Equation 12, the pressure drop across the CEE region (ΔP_{CEE}) is not a function of the flow rate. That is, (ΔP_{CEE}) is constant at the same LGR (F) irrespective of the total flow rates. In other words, it is proved in Equation 12 that the ΔP_{CEE} is constant for all SS-k_r measurements performed at different flow rates but with the same LGR.

However, the length of the CEE region (L_{CEE}) is not constant for all flow rates. Considering the constant ΔP_{CEE} for different total flow rates at the same LGR, the pressure drop across the core can be written as follows:

$$\Delta P_{core} = \frac{q_g\, \mu_g\, (L - L_{CEE})}{K k_{rg}(S_o{}^*) A} + \Delta P_{CEE} \tag{14}$$

In Equation 14, when applied to the results of an experiment, the values of L_{CCE}, $k_{rg}(S_o{}^*)$ and ΔP_{CEE} are unknown, which are going to be determined.

In a similar way, it can be shown that the "average liquid saturation" at the CEE region is also constant for different flow rates with the same LGR. That is, the average saturation is defined as:

$$\bar{S}_{o\,CEE} = \frac{\int_{L_{CCE}}^{L} S_o\, dx}{\int_{L_{CEE}}^{L} dx} \tag{15a}$$

which can also be written as follows, if Equation 7 is used:

$$\bar{S}_{o\,CEE} = \frac{\int_{L_{CEE}}^{L} S_o\, dx}{\int_{L_{CEE}}^{L} dx} = \frac{\int_{S_o}^{1-S_{gr}} \frac{S_o \frac{dP_c}{dS_o}\, dS_o}{\frac{1}{KA}\left(\frac{q_o\mu_o}{k_{ro}} - \frac{q_g\mu_g}{k_{rg}}\right)}}{\int_{S_o}^{1-S_{gr}} \frac{\frac{dP_c}{dS_o}\, dS_o}{\frac{1}{KA}\left(\frac{q_o\mu_o}{k_{ro}} - \frac{q_g\mu_g}{k_{rg}}\right)}} \qquad (15b)$$

$$= \frac{q_g \int_{S_o}^{1-S_{gr}} \frac{S_o \frac{dP_c}{dS_o}\, dS_o}{\left(\frac{q_o\mu_o}{k_{ro}} - \frac{q_g\mu_g}{k_{rg}}\right)}}{q_g \int_{S_o}^{1-S_{gr}} \frac{\frac{dP_c}{dS_o}\, dS_o}{\left(\frac{q_o\mu_o}{k_{ro}} - \frac{q_g\mu_g}{k_{rg}}\right)}} = \frac{\int_{S_o}^{1-S_{gr}} \frac{S_o \frac{dP_c}{dS_o}\, dS_o}{\left(F\frac{\mu_o}{k_{ro}} - \frac{\mu_g}{k_{rg}}\right)}}{\int_{S_o}^{1-S_{gr}} \frac{\frac{dP_c}{dS_o}\, dS_o}{\left(F\frac{\mu_o}{k_{ro}} - \frac{\mu_g}{k_{rg}}\right)}}$$

As shown in this equation, the average oil saturation in the CEE region ($\bar{S}_{o\,CEE}$) is also independent of flow rates and it is constant for all SS-k_r experiments performed at different flow rates with the same LGR (F). Therefore, the saturation equation for the core, considering the two separate regions, can be written as follows:

$$\overline{S_o}\,\mathrm{L} = S_o^{*}(L - L_{CEE}) + \bar{S}_{o\,CEE}\, L_{CEE} \qquad (16)$$

where $\overline{S_o}$ is the average wetting phase saturation inside the entire core, which is measured during the SS-k_r experiment, S_o^{*} is the wetting phase saturation in the unaffected zone, L_{CEE} is the length of the CEE region and $\bar{S}_{o\,CEE}$ is the average saturation in the CEE region. It should be noted that, in Equation 16, when applied to the results of a SS-k_r experiment, S_o^{*}, L_{CEE} and $\bar{S}_{o\,CEE}$ are again unknowns which are going to be determined.

During the experiments, the pressure drop across the core (ΔP_{Exp}) and the average saturation ($\bar{S}_{Exp}$) can be measured at each flow rate. It is noted that this measured average saturation ($\bar{S}_{Exp}$) is the average wetting phase saturation in the entire core ($\overline{S_o}$).

Assuming performing SS-k_r experiments at four different flow rates (with constant LGR), the following equations can be written for pressure and wetting phase saturations:

$$\begin{cases} \Delta P^1_{Exp} = \dfrac{q^1_g\ \mu_g\ (L - L^1_{CEE})}{K k_{rg}(S_o{}^*) A} + \Delta P_{CEE} \\ \Delta P^2_{Exp} = \dfrac{q^2_g\ \mu_g\ (L - L^2_{CEE})}{K k_{rg}(S_o{}^*) A} + \Delta P_{CEE} \\ \Delta P^3_{Exp} = \dfrac{q^3_g\ \mu_g\ (L - L^3_{CEE})}{K k_{rg}(S_o{}^*) A} + \Delta P_{CEE} \\ \Delta P^4_{Exp} = \dfrac{q^4_g\ \mu_g\ (L - L^4_{CEE})}{K k_{rg}(S_o{}^*) A} + \Delta P_{CEE} \end{cases} \quad (17)$$

and

$$\begin{cases} \bar{S}^1_{Exp} L = S_o{}^*\ (L - L^1_{CEE}) + \bar{S}_{CEE}\ L^1_{CEE} \\ \bar{S}^2_{Exp} L = S_o{}^*\ (L - L^2_{CEE}) + \bar{S}_{CEE}\ L^2_{CEE} \\ \bar{S}^3_{Exp} L = S_o{}^*\ (L - L^3_{CEE}) + \bar{S}_{CEE}\ L^3_{CEE} \\ \bar{S}^4_{Exp} L = S_o{}^*\ (L - L^4_{CEE}) + \bar{S}_{CEE}\ L^4_{CEE} \end{cases} \quad (18)$$

where L^1_{CEE}, L^2_{CEE}, L^3_{CEE}, L^4_{CEE},$S_o{}^*$, $k_{rg}(S_o{}^*)$,$\bar{S}_{CEE}$ and ΔP_{CEE} are unknowns. The above eight equations can be solved simultaneously for these unknowns. After solving the equations, the wetting phase saturation $S_o{}^*$ and non-wetting relative permeability $k_{rg}(S_o{}^*)$ are known. Thus, the only unknown value for plotting the relative permeability data is $k_{ro}(S_o{}^*)$. This value can be calculated using the Darcy law as follows. After solving the equations (Equation 17 and 18), the pressure drop across the CEE region is obtained. Therefore, the value of the pressure drop across the "unaffected zone" can be also calculated ($\Delta P_{unaf.} = \Delta P_{Exp} - \Delta P_{CEE}$). Having the pressure drop across the unaffected zone and the liquid rate, the $k_{ro}(S_o{}^*)$ can be easily calculated using Darcy law. Therefore, the corrected k_r data corresponding to a single LGR are obtained. The procedure should then be repeated for the next LGR. In the following sections, the proposed technique is evaluated, using both theoretical and experimental data.

4. Results and Discussion

CEE Correction by the Multi-Rate Method: Theoretical Data

In this section, the integrity of the proposed technique is evaluated using two sets of theoretically generated data. To achieve this aim, known functions of P_c and k_r data were employed in the corresponding analytical equation to simulate a steady-state two-phase displacement through a core. The theoretically generated experimental data (i.e. pressure drop (ΔP_{EXP}) from Equation 9, and average saturation ($\bar{S}_{Exp}$) from Equation

15) were then obtained. For generation of these data, the input parameters were selected in such way to have dominant end effects. In the next step, to evaluate the proposed technique, the generated experimental data (with CEEs) were used to predict the corrected k_r data. Finally, the corrected data obtained by the proposed method were compared with the actual known k_r functions. The predicted CEE length and pressure drop were also compared with the analytically calculated values. In this study, the imbibition k_r and P_c functions, shown in Figure 3 were used. Table 2 shows the PVT and the core properties used for this exercise.

Table 2 : Rock and PVT properties used in the numerical solution to generate experimental data.

Property	Test 1	Test 2
LGR	0.08	0.02
Gas flow rate (cc/hr)	4,5,11,15,30	5,11,15,25,50
Abs. Permeability (μD)	16	16
Area (cm^2)	11.4	11.4
Gas viscosity (cP)	0.0192	0.0192
Liquid viscosity (cP)	0.1268	0.1268
Core length (cm)	4.61	4.61
S_{oi} and S_{gr}	0.3 , 0.18	0.3 , 0.18

As mentioned before, using the k_r and P_c data in Figure 3 and input parameters shown in Table 2, the saturation profile at different flow rates can be numerically obtained using Equation 8. Figure 5 shows these obtained saturation profiles along the core for the two tests conducted at various LGRs. When LGR=0.08, the dimensionless CEE lengths (L_{CEE}/L) for the gas flow rates of 4, 5, 11, 15 and 30 are 0.689, 0.232, 0.218, 0.184 and 0.092, respectively. When LGR=0.02, the dimensionless CEE lengths (L_{CEE}/L) for the gas flow rates of 11, 15, 25 and 50 are 0.921, 0.676, 0.405 and 0.203 respectively. For gas flow rate of 5 cc/hr, the obtained L_{CEE} was greater than L which shows that the CEE region covers the entire core sample.

As mentioned before, at constant LGR the wetting phase saturation in the unaffected zone (S_o^*) is constant at all flow rates. In these results from numerical solutions, the S_o^* value at the higher LGR of 0.08 is 0.56 and at the lower LGR of 0.02, it is 0.45. It is clear that, by decreasing the LGR, S_o^* decreases.

Another point that should be noted here is the CEE length for different LGRs at the same flow rate. For example, when LGR=0.08, $L_{CEE}/L = 0.184$ for the gas flow rate of 15, while it is $L_{CEE}/L = 0.676$ for the same gas flow rate when LGR=0.02. It can be concluded that the CEE is more dominant at lower LGR. For example, in this case, the CEE has occupied the 18.4 % of the core length when LGR is 0.08, while it has occupied 67.6% of it, when LGR is equal to 0.02. Hence, at lower LGR, the CEE is more dominant. The same behaviour can be observed by comparing the simulated L_{CEE}/L for the flow rates of 5 and 11 cc/hr.

As mentioned above, from the numerical solution for a SS coreflood, the measured pressure drop and measured average saturation of wetting phase can be calculated. In other words, knowing the saturation profile along the core (from Equation 8), the pressure drop across the core can be calculated using Equation 9. In real SS k_r experiments, this pressure drop is usually measured across the core by the pressure transducers. The average saturation in the core can be also calculated using Equation 15. In real SS k_r experiments, this average saturation is obtained using the material balance. These data (pressure drop and average saturation) were used in the proposed procedure to obtain the corrected gas and oil k_r data. Table 3 and Table 4 show these parameters obtained from the numerical solutions.

Table 3: The pressure drop, measured k_{rg} and measured average saturation values in an artificial steady-state relative permeability experiment with LGR of 0.08.

q_g	**4 cc/hr**	**5 cc/hr**	**15 cc/hr**	**30 cc/hr**
$\Delta P_{Exp}\ (Psi)$	57.99	70.77	198.52	390.14
$k_{rg\ Exp}$	0.136	0.139	0.149	0.152
$\bar{S}_{Exp}$	0.574	0.571	0.564	0.562

Table 4: The pressure drop, measured k_{rg} and measured average saturation values in an artificial steady-state relative permeability experiment with LGR of 0.02.

q_g	**11 cc/hr**	**15 cc/hr**	**25 cc/hr**	**50 cc/hr**
$\Delta P_{Exp}(Psi)$	95.00	123.74	195.57	375.15
$k_{rg\ Exp}$	0.229	0.240	0.253	0.264
$\bar{S}_{Exp}$	0.478	0.470	0.462	0.456

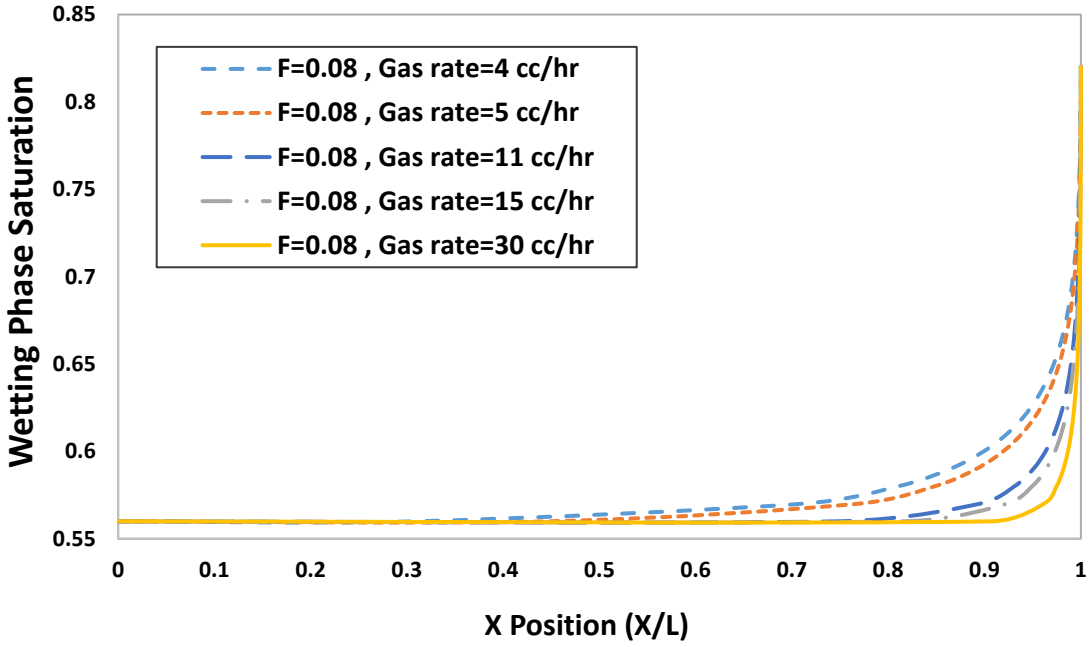

(a)

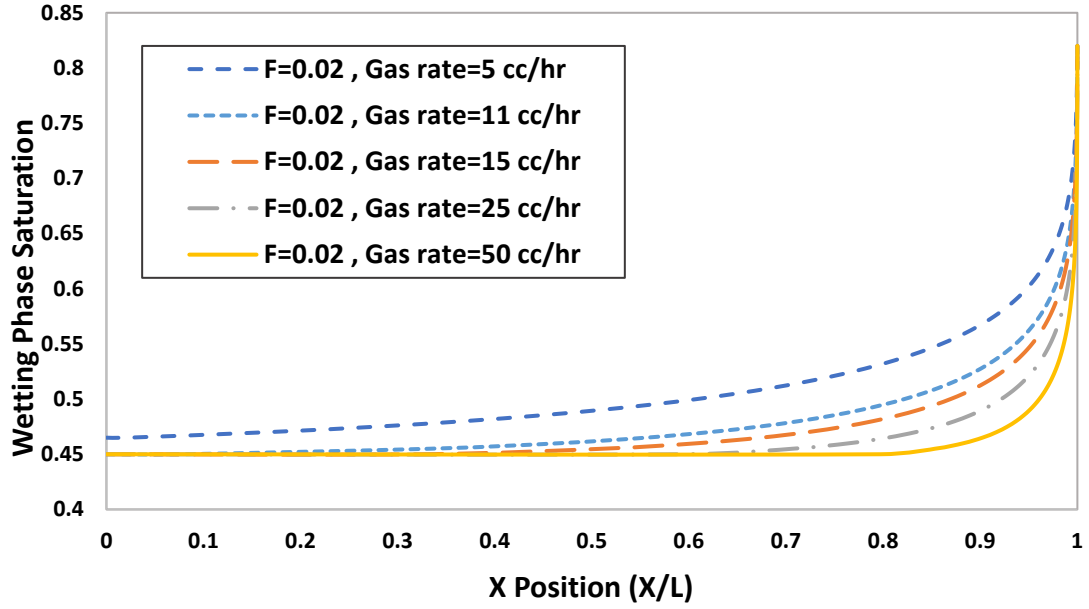

(b)

Figure 5 : The saturation profiles for two LGRs of (a) 0.08 and (b) 0.02 obtained from the simulation of core flooding experiments at five different flow rates.

For test 1 (LGR of 0.08), the artificial experimental data (ΔP_{Exp} and $\bar{S}_{Exp}$) shown in Table 3 were used in Equations 17 and 18 to obtain the unknowns, which are L^1_{CEE}, L^2_{CEE}, L^3_{CEE}, L^4_{CEE}, ${S_o}^*$, $k_{rg}({S_o}^*)$, $\bar{S}_{CEE}$ and ΔP_{CEE}. The data shown in Table 4 were also used with the same procedure to obtain the unknowns in test 2 (LGR of 0.02).

After using the proposed method for correction of CEE, the obtained results were compared with the actual values, as shown in Table 5. It should be noted that the actual data are obtained from the input k_r functions and the results of Eq. 8, 12 and 15b. As shown in this table, the predicted values are in good agreement with the actual data. In addition, benefiting from the proposed technique, some valuable information about the saturation profile and pressure drop along the core can be obtained. The wetting phase relative permeability, $k_{ro}(S_o^*)$, can be simply calculated by the Darcy equation when the length of the unaffected zone and the pressure drop across it are known. Figure 6 shows the gas and oil k_r obtained from the artificial experiment (with CEE) compared with the actual data (from the known function) and corrected data (using the proposed technique). In addition to two LGR of 0.08 and 0.25, artificial experimental data for LGR of 0.005 and 0.65 were generated and presented in this figure. It was aimed to evaluate the performance of the proposed method for the measured kr data close to the endpoints. As illustrated, the corrected values near the endpoint are acceptable enough compared to the actual data.

It has to be borne in mind that the measured k_r and saturation values can be corrected by the proposed method, as long as the experimental data for four different flow rates at each LGR are available. It should also be noted that, in this approach, it is necessary for the CEE region to be smaller than the core length. In other words, the core should not be entirely covered by the CEE region and the unaffected zone should be still available. Hence, if $L_{CEE} > L$ is obtained for a test, then a higher flow rate is required to shorten the CEE region.

Another advantage of this technique is that the proposed method can be applied to the experimental data before going to the next LGR. This means that, during the experiments, if $L_{CEE} > L$ is obtained for a set of flow rates at a specified LGR, the experiments can be repeated with higher flow rates before moving to the next LGR.

Table 5 : The actual and predicted values of CEE length, CEE pressure, wetting phase saturation and corresponding non-wetting relative permeability.

Parameter	Test 1 (LGR=0.08)			Test 2 (LGR=0.02)		
	Predicted	True value	Rel. Error (%)	Predicted	True value	Rel. Error (%)

L^1_{CEE}/L	0.7264	0.68911	5.41 %	0.9130	0.9211	0.88 %
L^2_{CEE}/L	0.5807	0.5513	5.33 %	0.6629	0.6755	1.87 %
L^3_{CEE}/L	0.1924	0.1838	4.68 %	0.3878	0.4053	4.32 %
L^4_{CEE}/L	0.0954	0.0919	3.78 %	0.1815	0.2026	10.41 %
$k_{rg}(S_o{}^*)$	0.1553	0.1550	0.21 %	0.2826	0.2758	2.47 %
ΔP_{CEE}	44.030	42.116	4.55 %	88.2944	88.7721	0.54 %
$\bar{S}_{CEE}$	0.5793	0.5803	0.17 %	0.4808	0.4805	~0%
$S_o{}^*$	0.5600	0.5600	0 %	0.4500	0.4507	~0%

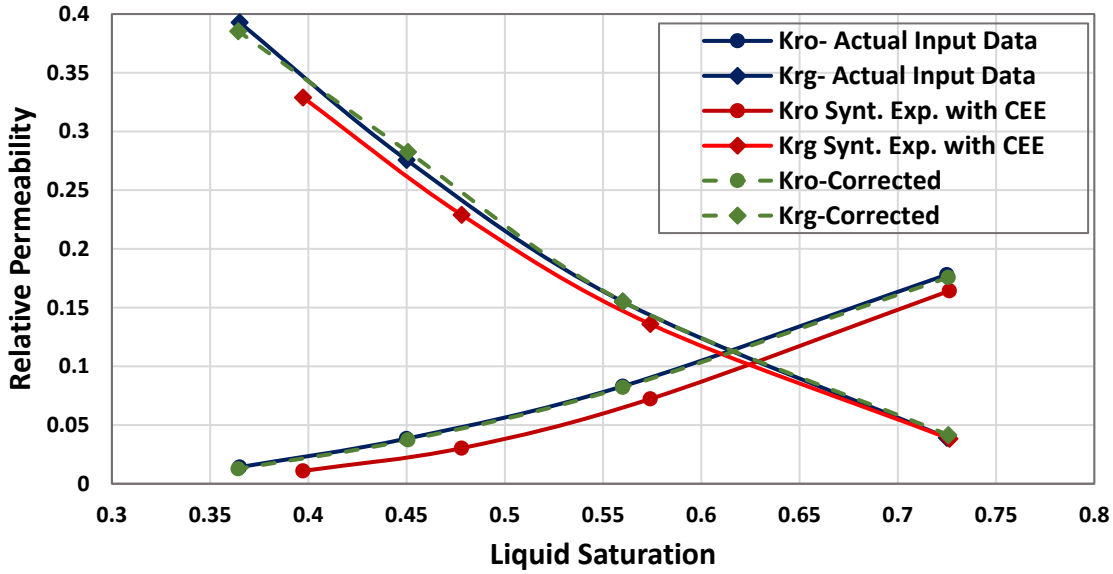

Figure 6 : The gas and oil relative permeability obtained from the artificial experiment compared with actual and corrected data using the proposed technique.

In Table 5, the pressure drop values across the CEE zone are also presented. As shown in Equation 12, this pressure is not a function of the flow rate. Hence, a certain value is obtained for each LGR, regardless of the injected flow rate. As mentioned before, Gupta and Maloney (2015) proposed a method to obtain this pressure drop (ΔP_{CEE}) from the non-zero intercept when plotting the measured pressures versus total flow rates (See Appendix I for more details). It is noted that, Gupta and Maloney assumed a constant CEE length to estimate the ΔP_{CEE} for each LGR, while as shown in this study, the CEE

lengths are different at different flow rates. As seen in Equation 14, the CEE length changes as flow rate changes, hence only plotting measured pressure versus flow rate will give a wrong value for ΔP_{CEE} (compare Equation 14 with Equation A-2 and A-3 in Appendix I). The results from following their procedure are shown in Figure 7. As indicated, the predicted ΔP_{CEE} by Gupta and Maloney (2015) method are 6.9, 18.9, 24.9 and -0.7 psi for tests with LGR of 0.08, 0.02, 0.005 and 0.65 respectively, while the true values are 42.1, 88.8, 157.9 and 4.12 psi.

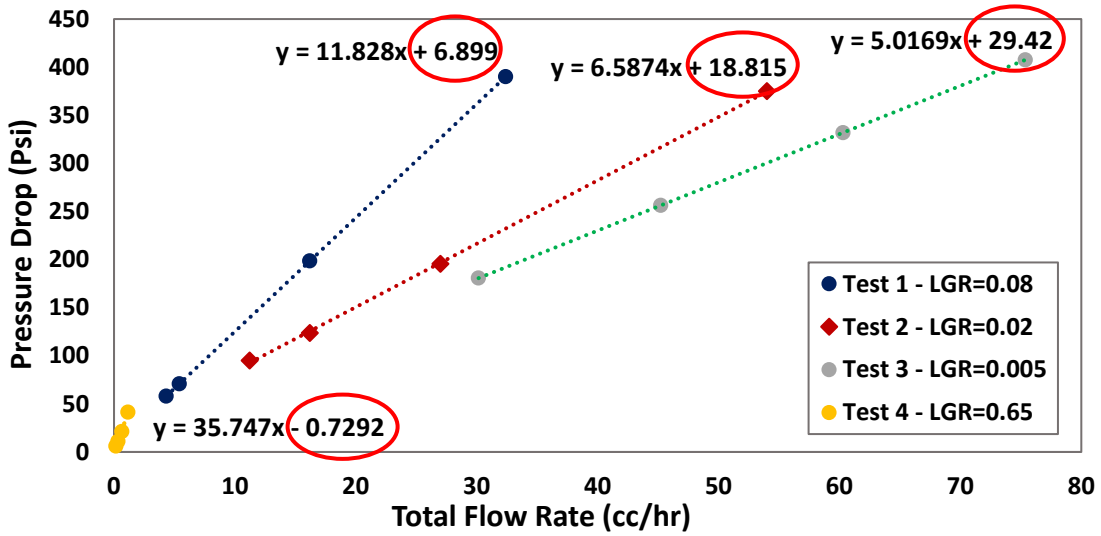

Figure 7 : Experimental pressure drops versus the total flow rates used to follow the intercept method proposed by Gupta and Maloney (2015). Based on their method, the non-zero intercept (red circles) gives ΔP_{CEE}.

CEE Correction by Rate Technique: Experimental Data

The relative permeabilities of an Eagle Ford shale sample were measured following the steady-state method explained earlier. For the Eagle Ford sample, four total flow rates of 10 cc/hr (equivalent to 1.6 m/day), 13 cc/hr (2.1 m/day), 16 cc/hr (2.5 m/day) and 20 cc/hr (3.2 m/day) were injected. As the SS-k_r experiments are tedious and time-consuming, the experiments were performed at two LGRs. To have a wider range of saturation, LGRs of 0.08 and 0.25 were selected. It is noted that, compared to conventional samples, the equilibrium state for unconventional rocks is achieved after a longer period of time. This is because of their ultra-low permeability and low injection rates used for displacement. To determine the end points, the relative permeability of gas and oil were measured at residual liquid and residual gas saturation, respectively.

The measured SS-k_r data of the Eagle Ford sample are shown in Figure 8. As illustrated, different relative permeability curves were obtained for different flow rates. As reported by many researchers [11, 12, 17], in the absence of CEE, the relative permeability data are not a function of flow rate. Therefore, it can be stated that these results have been affected by CEE. As explained before, for unconventional rocks, the capillary pressure is much higher compared to conventional samples. This high capillary pressure enhances the effect of CEE on measured data. In fact, the liquid hold-up at the core outlet depends on the competition of capillary forces and viscous force. In addition, as higher flow rates cannot be injected into such a tight matrix (injection at high rates results in a very unsustainably high pressure drop across the core) the viscous forces are small and the capillary forces are dominant. For example, for the core samples under study, the maximum practical injection rate is assumed to be 20 cc/hr, considering core physical properties and fluid viscosities at the experimental conditions. Injecting at higher flow rates creates a high pressure drop across the core, which results in an intensive stress change along the core. In addition, rock and fluid properties may change significantly when high pressure difference is applied across the core.

As can be seen in Figure 8, for almost all flow rates, different saturation and SS-k_r values were obtained, which confirms the presence of the capillary end effect (CEE). In these tests, and even at the highest injection flow rate, the CEE had a significant impact on the measured data. This discrepancy in the measured k_r increased as the LGR was decreased towards lower liquid saturation. It further confirms that the capillary end effect is the main reason for this observation. In other words, by reducing LGR, the end effects become more dominant. Here, at the left-hand side of Figure 8, significant differences are observed between the measured SS-k_r at the lower LGR which confirms the dominant influence of CEE on the measured data. In addition, as seen in this figure, the difference in the measured residual gas saturation and the SS-k_r value at different flow rates is negligible at higher LGR (right-hand side of Figure 8). Therefore, it is more necessary to correct the experimental k_r data for CEE at the lower LGRs.

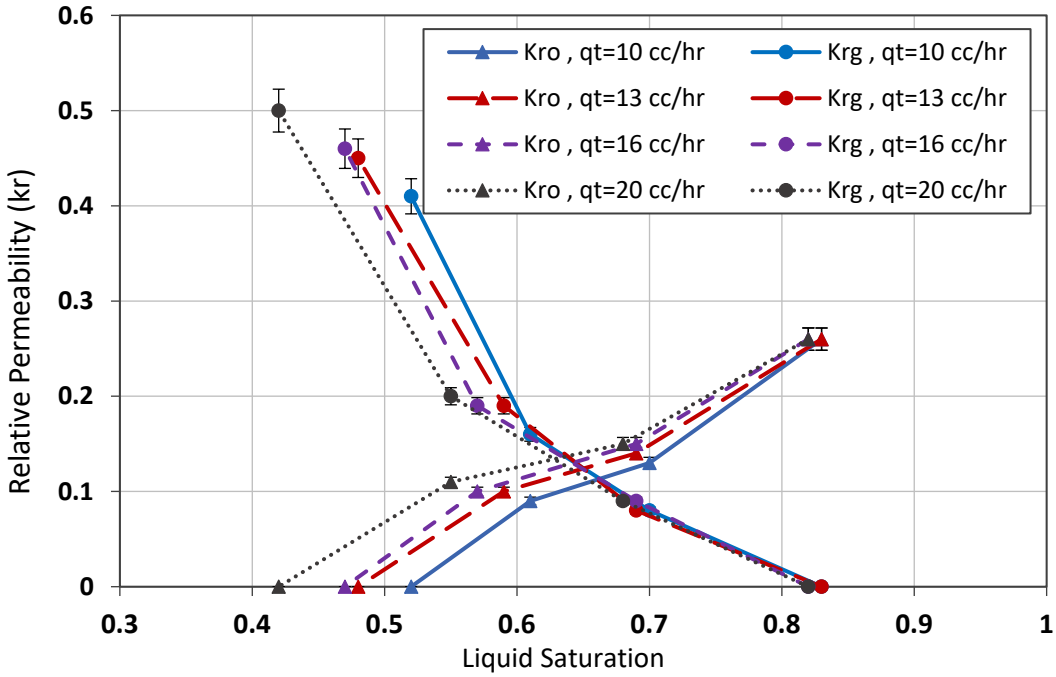

(a)

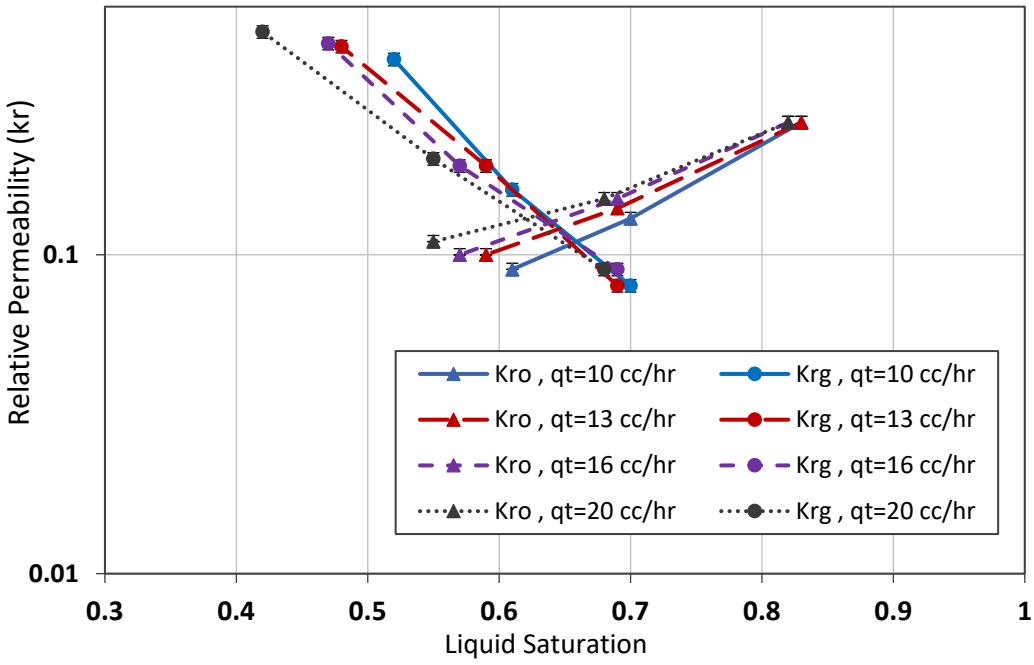

(b)

Figure 8 : Gas/oil SS-k_r data of Eagle Ford sample for different total flow rates measured at 1500 psi (corresponding to IFT of 5.5 mN/m) shown in (a) linear and (b) semi-log scale.

In addition to the verification by theoretical data, the developed technique was applied to the measured experimental data to correct the CEE. To this aim, the pressure drop and saturations obtained during SS-k_r measurements (shown in Figure 8) were used in

Equations 17 and 18 to estimate the CEE length, relative permeability data and the corresponding saturations for each LGR. As before, to solve the equations, a numerical solver in MATLAB with the Levenberg-Marquardt algorithm was used.

Table 6 presents the results obtained for all flow rates, measured at two LGRs of 0.08 and 0.25. As shown, the estimated CEE length (L_{CEE}) is longer for the lower flow rates, which confirms that the CEE decreases as the injection rate increases. In addition, as seen in this table, the CEE region covers a significant area of the Eagle Ford sample during the SS-k_r measurements. This confirms the prevailing effect of the CEE on the experimental data when measuring SS-k_r of Eagle Ford shale. It is also shown that the corrected gas k_r value is 0.28, which is 8% greater than 0.2, which was the value obtained at the highest flow rate. This means that the CEE may cause errors, even in measured k_r data with the highest possible flow rate.

Furthermore, at LGR of 0.25, a smaller CEE length was estimated compared to that at the same flow rate and LGR of 0.08. At LGR of 0.25, the corrected gas k_r is 0.11, which is 2 % higher than the value obtained at the highest flow rate. It also proves that the corrections are more necessary for the experimental data measured at lower LGRs. In addition, the wetting phase saturation in the unaffected zone was obtained at each LGR. As shown in Table 6, at LGR of 0.08, the wetting phase saturation ($S_o{}^*$) was 0.49, which is 6% smaller than the average saturation obtained at the highest flow rate. This difference is 3% at the highest LGR of 0.25. This further confirms the necessity of CEE correction for experimental data measured at lower LGR.

Table 6: The obtained CEE lengths, CEE pressures, wetting phase saturations and the corresponding non-wetting relative permeability values for the Eagle Ford shale sample.

LGR	Total Flow Rate (cc/hr)	ΔP_{Exp} (psi)	L_{CEE}	$k_{rg}(S_o{}^*)$	ΔP_{CEE} (psi)	$\bar{S}_{CEE}$	$S_o{}^*$
0.08	10	190.9	0.85	0.28	174	0.63	0.49
	13	212.0	0.74				
	16	249.1	0.59				
	20	307.1	0.41				
0.25	10	327.8	0.53	0.11	184	0.74	0.65
	13	410.0	0.43				
	16	463.9	0.42				
	20	572.7	0.37				

Using the estimated CEE length, the oil relative permeability can be calculated using the Darcy equation applied to the unaffected zone (i.e. non-CEE length), based on the oil viscosity and pressure difference. The corrected SS-k_r data are shown in Figure 9, together with the uncorrected values from the experiments. As shown, uncorrected experimental data give underestimated relative permeability values. In addition, liquid build-up due to the CEE causes higher wetting phase saturation along the core. However, for the Eagle Ford shale sample, the corrections were not required for the experimental data measured at residual gas saturation, as there were no significant changes at different rates.

As mentioned before, the proposed method can be applied to correct the experimental data as long as the CEE region is smaller than the core length. In other words, if the CEE region covers the entire core, the proposed technique cannot be applied and negative values will be obtained for the non-CEE length. This means that the viscous forces are not strong enough to compete with capillary end effect and thus the CEE region covers the entire core. Considering this point, it should be added that the proposed method cannot be applied to correct the experimental data of Eagle Ford shale obtained for LGR of less than 0.08, since the CEE region is extended all along the core. As shown in Table 6, at LGR of 0.08, the CEE zone extended up to 85% of the core length, at the total flow rate of 10 cc/hr. It is evident that at lower LGRs (towards the residual liquid saturation), the CEE covers the entire core length and the proposed technique cannot be applied. However, based on the corrections performed on the experimental data at LGRs of 0.25 and 0.08, a trend with major differences in k_r and wetting phase saturations is expected, shown as a green dotted line in Figure 9.

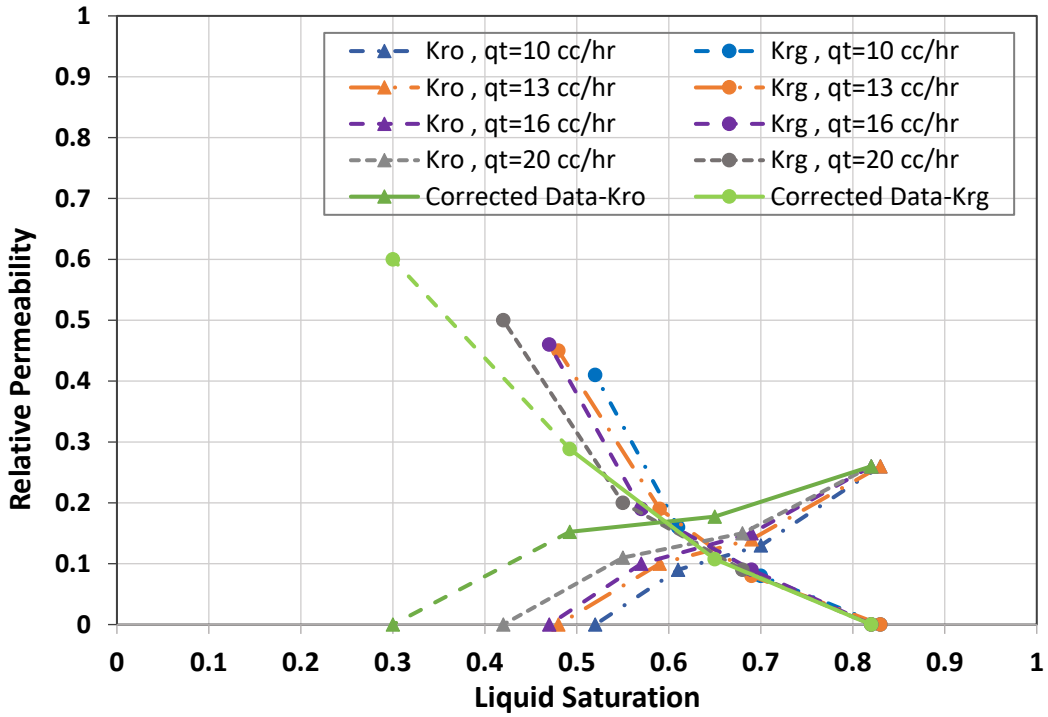

(a)

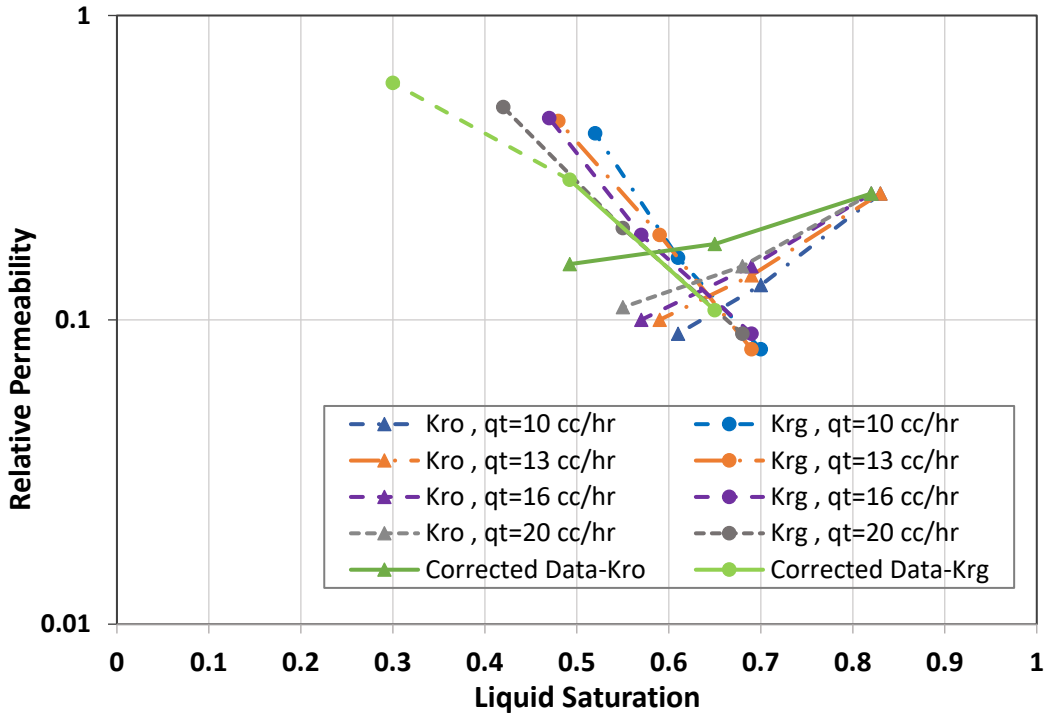

(b)

Figure 9 : Experimental and predicted relative permeability data measured on the Eagle Ford shale samples at 1500 psi (corresponding to IFT of 5.5 mN/m) shown in (a) linear and (b) semi-log scale.

5. Conclusions

In this study, a new technique was proposed to correct the steady state relative permeability (SS-k_r) data affected by capillary end effects (CEE). In the proposed technique, steady state displacements at four different flow rates are required to estimate the CEE length, oil/gas relative permeability, fluid saturations and pressure drop in the unaffected zone. It was mathematically shown that, for a constant LGR, the pressure drop and the average wetting phase saturation within the CEE region are constant and independent of flow rate.

In addition, the integrity of the proposed method was evaluated using series of artificially generated experimental data. For this purpose, a set of capillary pressure (P_c) and k_r data were assumed and used in the analytical solution of two-phase flow coupled with P_c. The analytical solutions were then used to generate artificial experimental data for pressure drop and average saturation during the SS-k_r measurements. The generated data were then utilised in the proposed technique to estimate the k_r data and the fluid saturations corrected for CEEs. In addition, the proposed technique was used to correct the SS-k_r data of a shale sample (Eagle Ford). The data from SS displacement experiments conducted at four different flow rates were used to obtain the corrected SS-k_r data. The following observations and conclusions can be drawn from this study:

- The simulation results of SS two-phase flow showed that the CEE is more significant during the SS-k_r experiment performed at lower LGR. In addition, the dominant role of the CEE increases as the injection rate is decreased.
- The proposed model was validated by artificially generated data. It was shown that the corrected SS-k_r data obtained by the proposed method were in good agreement with the actual known k_r data of the input.
- The SS-k_r data of the Eagle Ford shale showed a significant variation when measured at different injection rates. This variation was significant for lower LGR and decreased by increasing LGR. It was concluded that the CEE is the main reason for this observation, as a similar behaviour was shown in the results from the numerical solutions.
- Comparison of the measured k_r data and the corrected values showed that ignoring CEEs during SS-k_r measurements of tight and shale rocks can be highly erroneous.

- The proposed technique can be used to estimate reliable k_r data without any saturation profile measurement equipment, such as CT-scan or MRI. In addition, the proposed technique can be simply applied to the measured data during the experiment and, if required, the test can be repeated before going on to the next LGR.

LIST OF SYMBOLS

Nomenclature

A	area
K	absolute permeability
q	flow rate
S	saturation
F	liquid/gas flow rate ratio
P	pressure
L	length
x	distance
F	liquid gas flow rate ratio
S_o^*	wetting phase (oil) saturation
$\overline{S_o}$	average wetting phase (oil) saturation
IFT	interfacial tension
μ	viscosity

Subscript

g	gas
o	oil
c	capillary pressure
or	residual oil
gr	residual gas
ro	oil relative permeability
rg	gas relative permeability

out	outlet
Exp	experimental
CEE	capillary end effect
unaf	unaffected
t	total
r	relative

Abbreviations

CEE	capillary end effect
SS	steady state
LGR	liquid gas flow rate ratio

Acknowledgements

This study was conducted as a part of the Unconventional Gas and Gas-condensate Recovery Project at Heriot-Watt University. This research project is sponsored by: Daikin, Dong Energy, Ecopetrol/Equion, ExxonMobil, GDF, INPEX, JX-Nippon, Petrobras, RWE, Saudi-Aramco and TOTAL, whose contribution is gratefully acknowledged.

References

[1] M. Honarpour, S. Mahmood, Relative-permeability measurements: An overview, Journal of Petroleum Technology, 40 (1988) 963-966.
[2] Meng, Q., Liu, H., Wang, J. A critical review on fundamental mechanisms of spontaneous imbibition and the impact of boundary condition, fluid viscosity and wettability. Adv. Geo-energ. Res. 1 (2017), 1-17.
[3] J. Shen, J. Bae, An Automated Steady-State Relative Permeability Measurement System, paper SPE, 17217 (1987) 0.012-010.002.
[4] B. Maini, G. Coskuner, K. Jha, A Comparison Of Steady-State And Unsteady-State Relative Permeabilities Of Viscocities Oil And Water In Ottawa Sand, J Can Petrol Technol, 29 (1990).
[5] J. Richardson, J. Kerver, J. Hafford, J. Osoba, Laboratory determination of relative permeability, Journal of Petroleum Technology, 4 (1952) 187-196.
[6] G. Virnovsky, S. Skjaeveland, J. Surdal, P. Ingsoy, Steady-state relative permeability measurements corrected for capillary effects, in: SPE Annual Technical Conference and Exhibition, SPE 30541, Society of Petroleum Engineers, 1995.
[7] A. Al Hinai, R. Rezaee, L. Esteban, M. Labani, Comparisons of pore size distribution: a case from the Western Australian gas shale formations, Journal of Unconventional Oil and Gas Resources, 8 (2014) 1-13.
[8] G.R. Chalmers, D.J. Ross, R.M. Bustin, Geological controls on matrix permeability of Devonian Gas Shales in the Horn River and Liard basins, northeastern British Columbia, Canada, International Journal of Coal Geology, 103 (2012) 120-131.
[9] R. Gupta, D.R. Maloney, Intercept Method--A Novel Technique To Correct Steady-State Relative Permeability Data for Capillary End Effects, SPE Reservoir Evaluation & Engineering, (2016).
[10] M. Leverett, Capillary behavior in porous solids, Transactions of the AIME, 142 (1941) 152-169.
[11] J. Osoba, J. Richardson, J. Kerver, J. Hafford, P. Blair, Laboratory measurements of relative permeability, Journal of Petroleum Technology, 3 (1951) 47-56.
[12] L. Rapoport, W. Leas, Properties of linear waterfloods, Journal of Petroleum Technology, 5 (1953) 139-148.
[13] D.D. Huang, M.M. Honarpour, Capillary end effects in coreflood calculations, Journal of Petroleum Science and Engineering, 19 (1998) 103-117.
[14] S. Qadeer, K. Dehghani, D. Ogbe, R. Ostermann, Correcting oil-water relative permeability data for capillary end effect in displacement experiments, Springer, 1991.
[15] G. Virnovsky, K. Vatne, S. Skjaeveland, A. Lohne, Implementation of Multirate Technique to Measure Relative Permeabilities Accounting, in: SPE Annual Technical Conference and Exhibition, Society of Petroleum Engineers, 1998.
[16] A. Chen, A. Wood, Rate effects on water-oil relative permeability, in: Proceedings of the International Symposium of the Society of Core Analysts, Edinburgh, Scotland, 2001, pp. 17-19.
[17] M. Honarpour, F. Koederitz, A. Herbert, Relative permeability of petroleum reservoirs, C.R.C. Press, 1986, 1986.
[18] E. Withjack, Computed tomography for rock-property determination and fluid-flow visualization, SPE formation evaluation, 3 (1988) 696-704.
[19] S. Iglauer, S. Favretto, G. Spinelli, G. Schena, M.J. Blunt, X-ray tomography measurements of power-law cluster size distributions for the nonwetting phase in sandstones, Physical Review E, 82 (2010) 056315.
[20] D. Maloney, D. Wegener, D. Zornes, New x-ray scanning system for special core analyses in support of reservoir characterization, Paper SCA, 9940 (1999) 1-4.
[21] K. Romanenko, B.J. Balcom, An assessment of non-wetting phase relative permeability in water-wet sandstones based on quantitative MRI of capillary end effects, Journal of Petroleum Science and Engineering, 110 (2013) 225-231.

[22] R. Nazari Moghaddam, M. Jamiolahmady, Slip flow in porous media, Fuel, 173 (2016) 298-310.

Appendix I

Gupta and Maloney (2015) proposed the intercept technique to correct CEE during relative permeability measurements. The intercept method was proposed to correct CEE errors from both pressure and saturation measurements for each LGR. In this technique, several measurements of rate vs. pressure drop are required at the same LGR. The obtained trends in pressure drop vs. rate and saturation vs. rate will be used to correct the data for each single LGR. To correct the pressure data, one can start with Darcy's equation as follow

$$q_t\,(1-\mathrm{F}) = \frac{-Kk_{rw}A}{\mu_w L}\left(\Delta P_{theoritical\ without\ CEE}\right) \qquad \text{(A-1)}$$

where $\Delta P_{theoritical\ without\ CEE}$ is the pressure drop across the core without any capillary contribution to the pressure drop. $\Delta P_{theoritical\ without\ CEE}$ can be expressed as the difference between the experimental pressure drop across the core ΔP_{Exp} and the pressure drop resulting from the ΔP_{CEE}. Therefore,

$$q_t\,(1-\mathrm{F}) = \frac{-Kk_{rw}A}{\mu_w L}\left(\Delta P_{Exp} - \Delta P_{CEE}\right) \qquad \text{(A-2)}$$

Rearranging Eq. A-2 gives

$$\Delta P_{Exp} = \left(\frac{\mu_w L(1-F)}{Kk_{rw}A}\right) q_t + \Delta P_{CEE} \qquad \text{(A-3)}$$

Using the above concept, Gupta and Maloney proposed to obtain ΔP_{CEE} from the intercept of the plot of laboratory-measured pressure drop across the core (ΔP_{Exp}) and the injected total flow rate (q_t).

To correct the saturation data, they used the following overall saturation-balance equation for a given fractional-flow condition:

$$\mathrm{L}\,S_{w,avg} = (\mathrm{L}+x_i)S_{w,true} + x_i\,S_{w,CEE} \qquad \text{(A-4)}$$

where x_i is the length of CEE region, $S_{w,avg}$ is average water saturation, $S_{w,CEE}$ is average saturation of CEE region and $S_{w,true}$ is actual water saturation as shown in Figure A-1.

They defined CEE-length factor as $\beta = \frac{x_i}{L}$ and proposed the following equation as a reliable concept to correct the saturations.

$$\beta = \frac{\Delta P_{CEE}}{\Delta P_{Exp} - \Delta P_{CEE}} \quad \text{(A-5)}$$

Rearranging Equation A-4 and use of Equation A-5 gives the expression

$$\frac{1}{(1-\beta)} S_{w,avg} = S_{w,CEE} \frac{\beta}{(1-\beta)} + S_{w,true} \quad \text{(A-6)}$$

Based on Equation A-6, CEE-corrected saturation (i.e. $S_{w,true}$) is the intercept of the plot of $(\frac{1}{(1-\beta)} S_{w,avg})$ and $(\frac{\beta}{(1-\beta)})$.

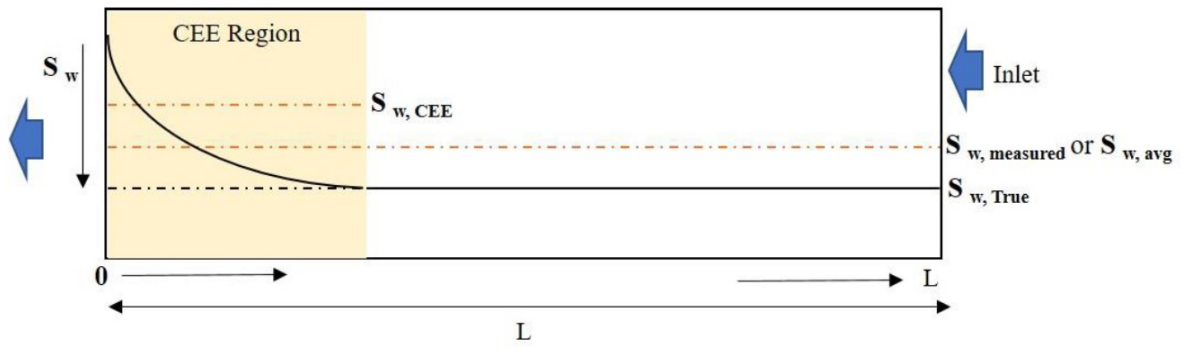

Figure A-1: Schematic of water saturation highlighting the average water saturation ($S_{w,avg}$), average saturation of CEE region ($S_{w,CEE}$), and asymptotic water saturation ($S_{w,true}$) presented by Gupta and Maloney (2015).